Title

Broadcasting of Cortical Activity to the Olfactory Bulb

Journal

Cell Reports, 10(7)

ISSN

2639-1856

Authors

Boyd, Alison M
Kato, Hiroyuki K
Komiyama, Takaki
et al.

Publication Date

2015-02-01

DOI

10.1016/j.celrep.2015.01.047

Peer reviewed

Published in final edited form as:
Cell Rep. 2015 February 24; 10(7): 1032–1039. doi:10.1016/j.celrep.2015.01.047.

Broadcasting of cortical activity to the olfactory bulb

Alison M. Boyd[1], **Hiroyuki K. Kato**[1], **Takaki Komiyama**[1,2,3], and **Jeffry S. Isaacson**[1,*]

[1]Center for Neural Circuits and Behavior and Department of Neurosciences, University of California, San Diego, La Jolla, CA 92093, USA

[2]Neurobiology Section, Division of Biological Sciences, University of California, San Diego, La Jolla, CA 92093, USA

[3]JST, PRESTO University of California, San Diego, La Jolla, CA 92093, USA

Summary

Odor representations are initially formed in the olfactory bulb, which contains a topographic glomerular map of odor molecular features. The bulb transmits sensory information directly to piriform cortex where it is encoded by distributed ensembles of pyramidal cells without spatial order. Intriguingly, piriform cortex pyramidal cells project back to the bulb, but the information contained in this feedback projection is unknown. Here we use imaging in awake mice to directly monitor activity in the presynaptic boutons of cortical feedback fibers. We show that the cortex provides the bulb with a rich array of information for any individual odor and that cortical feedback is dependent on brain state. In contrast to the stereotyped, spatial arrangement of olfactory bulb glomeruli, cortical inputs tuned to different odors commingle and indiscriminately target individual glomerular channels. Thus, the cortex modulates early odor representations by broadcasting sensory information diffusely onto spatially ordered bulbar circuits.

Introduction

Sensory regions of neocortex receive information from the thalamus and make corticothalamic feedback projections that serve to modify thalamic sensory processing (Briggs and Usrey, 2008). In the visual, auditory, and somatosensory systems the connectivity of feedback projections onto thalamic neurons is linked to the tuning preferences of the cortical cells involved and there is a high degree of reciprocity between topographically aligned areas of cortex and thalamus (He, 2003; Murphy et al., 1999; Temereanca and Simons, 2004). The olfactory system is unique in that sensory information bypasses the thalamus such that the primary olfactory (piriform) cortex receives sensory input directly from the olfactory bulb, the first brain region in which odor information is processed. Similar to corticothalamic pathways, olfactory cortex pyramidal cells send dense

*Correspondence: jisaacson@ucsd.edu (J.S.I.).

projections back to the olfactory bulb (Luskin and Price, 1983). However, the information sent back to the bulb from the piriform cortex (PCx) and the functional topography of feedback input has not been established.

The olfactory bulb contains a highly ordered spatial map of odorant molecular features. This reflects the fact that olfactory sensory neurons (OSNs) expressing only one out of ~1000 odorant receptors converge input onto two unique glomeruli (out of ~2000) in each olfactory bulb (Mombaerts et al., 1996). Within each glomerulus, OSNs contact a unique set of principal mitral cells that project sensory information to the PCx. Ultimately, different odors activate distinct glomerular channels generating a stereotyped topographic map of odor space in the olfactory bulb (Soucy et al., 2009). In contrast, studies of sensory representations in the PCx reveal that odors are encoded by dispersed and overlapping populations of pyramidal cells without obvious spatial order (Stettler and Axel, 2009). Thus, the initial stereotyped and topographic representation of olfactory information in the bulb is discarded and replaced by a distributed ensemble coding strategy in the cortex.

Mitral cell odor responses are not solely determined by the excitatory input they receive from individual glomeruli. This reflects the fact that mitral cell activity is regulated by a variety of local GABAergic interneurons, the most prominent of which are periglomerular cells, which contact the apical dendritic tuft of mitral cells, and granule cells that inhibit mitral cell lateral dendrites (Shepherd et al., 2004). The axonal projections of PCx pyramidal cells are particularly dense in the granule cell layer and also surround but do not extend into glomeruli (Matsutani, 2010), suggesting that bulbar interneurons are the major targets of cortical feedback. Consistent with this idea, granule and periglomerular cells are strongly excited by cortical feedback projections (Boyd et al., 2012; Markopoulos et al., 2012) and activation of PCx amplifies odor-evoked mitral cell inhibition (Boyd et al., 2012). Thus, PCx can effectively gate odor-evoked olfactory bulb output and directly regulate the sensory input it receives.

Although cortical feedback has a strong impact on olfactory bulb circuits, the nature of the information contained in feedback projections is unclear. What is the olfactory cortex trying to “tell” the olfactory bulb? To address this question, we express the genetically-encoded Ca^{2+} indicator GCaMP6s (Chen et al., 2013) in PCx and use 2-photon imaging to study the activity of pyramidal cell axonal boutons in the olfactory bulb of awake mice. We determine the sensory information within long-range cortical projections and show its modulation by brain state. In contrast to corticothalamic pathways, we show that the targeting of feedback input ignores local topographic order allowing the cortex to broadcast sensory information widely across olfactory bulb circuits.

Results

We co-injected two different viral vectors to express GCaMP6s (AAV 2/9-syn-GCaMP6s) and the activity-independent reporter TdTomato (AAV 2/9-syn-tdTomato) in PCx pyramidal cells (Fig. $1A_1$, Supplemental Fig. 1). To visualize cortical feedback inputs, we subsequently imaged the ipsilateral olfactory bulb of awake, head-fixed mice through a chronically implanted glass window ((Kato et al., 2012), Fig. $1A_1$). The tdTomato signal was used for

registration of image time series as well as estimation of residual movement-related artifacts that we used to establish the GCaMP response threshold (Experimental Procedures, Supplemental Fig. 1). The labeling pattern in the olfactory bulb was consistent with previous reports of cortical projections (Boyd et al., 2012; Markopoulos et al., 2012): labeled axons and boutons were densest in the granule cell layer and prominent in the glomerular layer (Fig $1A_2$). We never observed labeling in local bulbar neurons, indicating that signals arise exclusively from long-range cortical projections.

We resolved individual micrometer-sized varicosities in vivo (Fig. $1A_2$) and assume that each represents a single presynaptic bouton (Petreanu et al., 2012). Co-injection of tdTomato and GCaMP led to co-expression of the two fluorescent proteins in the same fibers and boutons as well as non-overlapping expression in separate populations of fibers. We first examined sensory-evoked activity in the awake state by testing the responses of individual boutons to a panel of seven structurally diverse, monomolecular odorants (each at 100 ppm). Individual boutons within a single field of view (85x85 or 128×128 μm) revealed diverse responses (Supplemental Movie 1). In both the granule cell and glomerular layer, odor application (4 s) elicited increases in the activity of single boutons (measured as dF/F). Individual boutons showed a range of odor tuning, from being odor selective to responding to all tested odors. Furthermore, immediately adjacent boutons could have divergent tuning properties (Fig. 1B). The time course of odor-evoked activity varied from phasic responses to long-lasting activity that persisted for many seconds after odor delivery. We observed odor-evoked decreases in fluorescence (negative dF/F responses) indicating that sensory stimulation could also suppress the basal activity of feedback projections. Pairwise correlation analysis of boutons indicated that, on average, a minimum of 20.5±2 distinct axons (n=23 fields) contributed to each imaging field (Supplemental Fig. 2). There were no obvious differences between the properties of boutons in the two bulb layers (Supplemental Fig. 3, total boutons=4948, n=9 granule cell layer fields, 18 glomerular layer fields, 16 mice) and results were pooled for further analysis.

Excitatory and suppressive responses had different temporal dynamics; while the onset time of excitation included both on- and off-responses, suppressive activity was more time locked to odor onset (Fig. 1C). Boutons with odor-evoked increases in activity (21.2% out of 5353 total boutons) were more prevalent than those showing suppression (11.5%) and boutons with both excitatory and suppressive responses to different odors were rare (2.4%, Fig. $1D_1$). The fraction of odor-activated boutons we observe (~24%) is consistent with a previous PCx imaging study using five odors that found ~35% of layer 2 neurons are odor responsive (Stettler and Axel, 2009). Since the optical detection of odor-evoked suppression relies on substantial basal activity, we are potentially underestimating decreases in feedback input. Nonetheless, the tuning properties of boutons in which odors elicited increases or decreases in activity were similar: ~50% of boutons responded with specificity (to two or fewer of the seven odors). Although most boutons (~65%) were unresponsive to the tested odors, virtually all boutons lacking odor-evoked responses (>90%) displayed spontaneous activity indicating they were functional. Thus, the majority of feedback inputs are likely to respond to odors more selectively. We considered the possibility that some odors may be more represented by cortical feedback than others. However, across the population of responsive boutons tested with the same panel of odors (n=554 boutons, 1674 responses), each odor

was virtually identical in terms of its likelihood of eliciting excitatory responses (Fig. 1D_2). Similar results were observed using a larger panel of 14 odors (Supplemental Fig. 3). Together, these results indicate that individual odors are represented equally by PCx feedback and that local regions of the bulb receive input from fibers with diverse response properties.

Olfactory bulb activity is dependent on brain state (Rinberg et al., 2006). Indeed, the transition from the awake to anesthetized condition strongly reduces bulbar interneuron activity and enhances odor-evoked mitral cell output (Cazakoff et al., 2014; Kato et al., 2012; Wachowiak et al., 2013). How does cortical feedback input respond to this change in brain state? To address this, we imaged the same boutons in the awake and anesthetized state. Anesthesia caused a marked decrease in both spontaneous and odor-evoked cortical feedback (Fig. 2A,B). Relative to the awake condition, anesthesia reduced the number of boutons responding with odor-evoked excitation and suppression by 39.6% and 48.8%, respectively (n= 6 imaging fields from 4 mice). During anesthesia the strength of excitatory responses was reduced ($p<0.001$, Kolmogorov-Smirnov (KS) test, Fig. 2C_1) and excitation became more narrowly tuned (Fig. 2C_2). These effects on odor-evoked responses were indistinguishable with ketamine and urethane (Supplemental Fig. 3), two chemically distinct anesthetics, suggesting that the differences in bouton activity reflect changes in brain state rather than pharmacological actions of the drugs. Furthermore, the duration of odor-evoked excitatory activity became markedly briefer in the anesthetized state (decay time awake = 4.2±0.2 s, anesthetized = 3.1±0.2 s, $p<0.001$, KS test, Fig. 2$D_{1\text{-}2}$) while the duration of suppressive responses was slightly enhanced (decay time awake = 2.3±0.1 s, anesthetized = 2.6±0.1 s, $p=0.001$, KS test, Fig. 2$D_{3\text{-}4}$). Overall, these results indicate that wakefulness enhances PCx feedback input to olfactory bulb circuits.

We next considered the functional organization of cortical projections within the olfactory bulb. Do feedback inputs adopt the topographic organization of the bulb such that the tuning of cortical inputs matches that of their target region? Or do they retain the diffuse and overlapping nature of odor representations found within the PCx itself? The observation that boutons with different tuning properties closely intermingle (Fig. 1B) suggests that cortical inputs do not transmit sensory information in a strict, spatially segregated manner. We tested this by examining whether boutons with the same odor preference are spatially clustered within our imaging fields (85×85 or 128×128 μm), each of which are on the scale of a radially oriented glomerular column (~100 μm diameter, (Willhite et al., 2006)). We made maps of bouton odor preference (the odor eliciting the strongest excitatory response) within a field (Fig. 3A_1) and measured the pairwise distance between all boutons with the same (matched) or different (mismatched) odor preference. If boutons with the same odor preference cluster, the distance between boutons with matching preferences should be less than those that are mismatched. However, for granule cell and glomerular layer fields with at least 30 responsive boutons, the average distance between matched or mismatched boutons was nearly identical (Fig. 3A_2, 3B, matched= 55.0±1.5 μm, mismatched=56.9±1.7 μm, $p=0.26$, Wilcoxon signed-rank test, n=22 fields). Similarly, we found no difference when we compared the distance between boutons based on the number of odors eliciting responses (tuning broadness, matched= 55.5±1.9 μm, mismatched=56.6±1.4 μm, $p=0.91$, Wilcoxon signed-rank test). Furthermore, there was no relationship between distance and the

tuning similarity (Soucy et al., 2009) of boutons (Supplemental Fig. 4). Thus, for bulb domains on the scale of individual glomeruli, cortical feedback does not appear to provide input in a spatially segregated fashion.

Another simple test of spatial organization is to ask whether boutons responsive to a particular odor are overrepresented within our imaging fields. Therefore, for all excitation responsive odor-bouton pairs in each imaging field (n=22), we rank ordered the seven odors by their probability of eliciting a response. On average, response probabilities within a field ranged from 20.0±0.5% (most preferred odor) to 7.6±0.6% (least preferred odor, Fig. 3C). If a field had an infinite number of odor-bouton response pairs, each odor should have a 14.3% (1/7) probability of contributing a response if odor responses are randomly distributed. However, the number of odor responses per field is limited and some odors may be more represented than others in each imaged field simply by chance. Indeed, given the number of odor-bouton response pairs we measured per field (range: 23 to 406 response pairs), our results are consistent with those expected due to random subsampling from a distribution of equal response probabilities (Fig. 3C). Thus, boutons activated by specific odors are not overrepresented on a glomerular spatial scale, suggesting that the targeting of feedback input lacks a segregated spatial order.

We took advantage of feedback projections in the glomerular layer to directly test if cortical boutons are co-tuned with the glomeruli they target. We first used intrinsic signal optical imaging to map glomerular activity (Rubin and Katz, 1999) in response to three odors (Fig. 4A,B_1) and then imaged bouton responses at the base of selected glomeruli. Immediately before 2-photon imaging, the red fluorophore Texas red dextran was injected i.v. (Fig. 4A). We visualized labeled blood vessels to align imaging fields to the surface vasculature and glomeruli observed during intrinsic signal imaging (Fig. 4B_1, B_2). If cortical projections are organized based on the odor map inherent to the olfactory bulb, boutons should show a preference for the odors activating their overlying glomeruli. However, beneath odor-specific glomeruli (n=9) we found boutons activated by each of the three of the odors (Fig. 4$B_{1\text{-}4}$). Furthermore, the probability of bouton responses to a given odor was similar whether the 2-photon imaging field was beneath the glomerulus activated by that odor (“Field 1”, Fig. 4B_3, B_4) or beneath glomeruli unresponsive to the odor (“Field 2”, Fig. 4B_3, B_4). Overall, for each of the three odors tested, odor-evoked bouton activity was unrelated to the overlying glomerular odor map (n=9 fields beneath active glomeruli, 6 fields beneath non-active glomeruli, n=3 mice, Fig. 4C). Similar results were obtained using seven odors and more imaging fields tiling the dorsal olfactory bulb (Supplemental Fig. 5). Taken together, our results indicate that cortical fibers transmit odor-evoked feedback input diffusely over the olfactory bulb without any obvious spatial segregation.

Discussion

In this study we use in vivo Ca^{2+} imaging to reveal the information contained within cortical feedback projections to the olfactory bulb. We show that PCx provides the bulb with diverse input: odors cause pyramidal cells to increase or decrease their feedback in a manner ranging from odor selective to apparently un-tuned. Compared to the anesthetized condition, wakefulness enhances both the magnitude and duration of excitatory cortical feedback,

indicating that the cortical control of olfactory bulb circuits is dependent on brain state. Furthermore, although olfactory bulb circuits are spatially arranged to form a stereotyped odor map, PCx projections provide feedback input in a diffuse, intermingled fashion.

Cortical feedback inputs directly excite olfactory bulb interneurons and facilitate mitral cell inhibition (Boyd et al., 2012; Markopoulos et al., 2012). We found that odors elicit both increases and decreases in cortical feedback activity and that the PCx transmits a heterogeneous array of odor information to the bulb. For example, although the majority of feedback projections show odor-specific changes in activity, others appear to be "generalists" that simply signal the presence of any odor. Our results are similar to those found using electrophysiological recordings of layer 2/3 PCx cells in awake mice (Zhan and Luo, 2010). This suggests that cortical feedback does not arise from a distinct subpopulation of pyramidal cells and that it may provide the bulb with a readout of overall PCx activity. In addition, while PCx feedback can be time locked to odor onset, responses can also be quite delayed and even persist long after the odor is present. The wide variety in response features indicates that PCx feedback exerts complex and non-uniform effects on the olfactory bulb interneurons underlying mitral cell inhibition. Interestingly, local inhibition is proposed to enhance odor discrimination by decorrelating mitral cell activity patterns (Arevian et al., 2008; Wiechert et al., 2010). Heterogeneous odor-evoked patterns of feedback input could allow PCx to contribute to the decorrelation of mitral cell activity and thus enhance the discriminability of input it receives from the olfactory bulb.

Odor coding in the olfactory bulb differs between the awake and anesthetized brain state, namely, mitral cell odor representations are sparser and more temporally dynamic during wakefulness (Kato et al., 2012; Rinberg et al., 2006; Wachowiak et al., 2013). These changes lead to a marked improvement in the discriminability of mitral cell odor representations (Kato et al., 2012). Intriguingly, despite the fact that sensory input to PCx is sparser, we find that wakefulness increases spontaneous activity as well as the strength and duration of odor-evoked excitatory cortical feedback. This suggests that cortical circuits are flexible and that PCx output can adapt to brain state-dependent changes in sensory input. What can explain the opposing changes in mitral cell activity and PCx feedback? Interestingly, wakefulness strongly increases the activity of olfactory bulb interneurons (Cazakoff et al., 2014; Kato et al., 2012; Wachowiak et al., 2013). For example, granule cells are predominantly inactive in the anesthetized state, but have high amounts of spontaneous activity and more broadly-tuned odor responses during wakefulness (Cazakoff et al., 2014; Kato et al., 2012). One explanation for the opposite changes in PCx and mitral cell activity is that brain state-dependent changes in interneuron activity are directly inherited from their PCx feedback input. Indeed, increased PCx feedback, acting to enhance the activity of local interneurons, could account for sparse mitral cell odor representations during wakefulness. Thus, modulation of PCx feedback may be a major factor regulating the state dependence of mitral and granule cell activity.

We show that PCx feedback inputs responding to different odors are dispersed throughout the granule cell and glomerular layer in a diffuse and overlapping fashion. Indeed, glomeruli tuned to specific odors are surrounded by feedback projections that transmit information regarding distinctly different odors. Thus, on the spatial scale of individual glomeruli, we

find no evidence that feedback inputs and their olfactory bulb targets are co-tuned or that feedback is targeted with odor selectivity. We cannot exclude the possibility that a diffuse spatial organization of feedback occurs on a much larger scale, for example between dorsal and ventral regions of the olfactory bulb. Our findings differ from a recent imaging study using GCaMP to examine the properties of feedback projections from the anterior olfactory nucleus (AON), an anterior subdivision of the olfactory cortex (Rothermel and Wachowiak, 2014). Imaging of the dorsal olfactory bulb suggested that individual odors could generate odor-specific patterns of activity. Unlike PCx, the AON receives olfactory bulb input that is topographically-organized (Ghosh et al., 2011; Miyamichi et al., 2011) raising the possibility that AON feedback is uniquely co-tuned with that of its target region.

Our results suggest that PCx feedback inputs broadcast odor information diffusely onto spatially ordered bulbar circuits. Thus, in contrast to the proposed “egocentric” enhancement of thalamic activity generated by visual, auditory, and somatosensory cortical feedback (Briggs and Usrey, 2008), PCx inputs are unlikely to selectively amplify the activity of mitral cells sharing the same tuning properties. Since PCx inputs target interneurons and drive mitral cell inhibition (Boyd et al., 2012), cortical feedback may regulate olfactory bulb output on a more global scale. Cortical feedback has been suggested to modulate the gain of thalamic output during brain states associated with attention (McAlonan et al., 2008) and the transition between sleep and wakefulness (Steriade, 2005). Feedback projections from the PCx may contribute a similar gain control function for the initial processing of odor representations in the olfactory bulb.

Experimental Procedures

Animals

Experiments followed approved national and institutional guidelines for animal use. We used either C57BL/6 wild type or Ntsr1-cre mice (Tg(Ntsr1-cre)209Gsat) that express Cre recombinase selectively in olfactory cortex pyramidal cells (Boyd et al., 2012). For the majority of experiments, we injected AAV 2/9-syn-GCaMP6s into the PCx of adult (≥40 days old) C57BL/6 mice at three locations (100 nl/site). We used similar injections of AAV2/9-FLEX-syn-GCaMP5G for conditional expression in a subset of Ntsr1-cre mice. AAV 2/9-syn-tdTomato was co-injected (50 nl/site) in a subset of mice to determine the effects of residual motion. Results were similar using GCaMP6s and GCaMP5G, thus all data were pooled. Coordinates of the injections sites, measured from the intersection of the midline and bregma were (in mm: anterior, lateral, depth): (2.6, 1.8, 4.2), (2.0, 2.0, 4.2), (1.9, 2.8, 4.6). All viruses were from U. Penn. Vector Core. Window implantations were performed as described previously (Kato et al., 2012) and mice recovered for >2 weeks before imaging.

Odor Stimulation and 2-Photon Imaging

Odors (Sigma) were diluted in mineral oil to a concentration of 200 ppm. An olfactometer mixed saturated odor vapor with filtered air 1:1 for a final concentration of 100 ppm. Each odor was applied (4 s duration, 1 min interval) for 5-10 trials. Every experiment included a

mock trial of air application used for receiver-operator characteristic analysis to establish response threshold.

GCaMP and tdTomato were excited at 920 nm (MaiTai, Newport) and images (512 × 512 pixels) were acquired with a microscope (Thorlabs) and 16x objective (Nikon) at ~15 Hz. Images were acquired from the glomerular (50-150 μm below the surface) or granule cell layer (300-400 μm below the surface). In a subset of experiments, mice were anesthetized with ketamine/xylazine (100 mg/kg and 8 mg/kg, respectively) or urethane (1.5 g/kg). Tail vein injections of Texas red dextran (70,000 MW, Invitrogen, 75-100 μl of a 5% v/v solution in PBS) were used to visualize vasculature.

Data Analysis

Lateral motion was corrected by cross correlation-based image alignment (Turboreg, ImageJ). We estimate the lateral motion, using frame-by-frame motion correction, to be <2.9 μm in 90% of frames. Regions of interest (ROIs) corresponding to individual axonal boutons were manually drawn based on the image obtained by averaging all frames collected during a 60 s trial for each odor. The time-varying baseline fluorescence trace was estimated by smoothing inactive portions of the trace as described previously (Peters et al., 2014). For each odor response, the trace was smoothed (15 frame sliding window average) and normalized by the baseline.

Using a response detection period of 10 s beginning with the onset of odor application, ROIs were classified as having an excitatory response to an odor if dF/F increased by 2.6X standard deviation (SD) of the baseline for 10 continuous frames, both in the average trace and in ≥ 50% of individual trials. This threshold was chosen to yield a false positive (FP) rate (estimated from air trials) of 9.5%. In addition, all responses had to be ≥20% dF/F, to avoid FPs caused by residual motion (Supplemental Fig. 1). Two separate, independent criteria were used for detecting inhibition. The first was a ≥60% reduction in the SD relative to baseline. The second was a ≥20% decrease in dF/F lasting ≥2 seconds (FP rate= 9.1%). Average response time course was derived by aligning responses to their 50% rise time and decay time was calculated from the time to 0.37 of peak amplitude. For analysis of response amplitude, the maximum dF/F value of the average trace (5-10 trials) during the response detection window was used.

For analysis of boutons based on matched or mismatched response properties, we used correlation analysis to select one bouton from axons contributing multiple boutons. This is due to the fact that spacing between boutons along the same fiber can be very small (<5 μm), yielding a disproportionately small distance between boutons with matching response properties. We performed simulations to investigate whether the observed distribution of odor response probabilities could be explained by subsampling from a distribution in which each odor had an equal probability of eliciting a response. Simulations were performed by subsampling from a random distribution of 10000 values (integers 1 through 7). We determined the distributions expected using the smallest and largest numbers of observed odor-response pairs. We confirmed that our measured value for the most preferred odor response probability could be explained by random subsampling by using the sample size of

the experiments, determining the average probability for the preferred odor, and repeating this 10000 times.

Intrinsic Imaging

Intrinsic images were acquired using a tandem lens macroscope and 12 bit, CCD camera (CCD-1300QF, VDS Vosskühler) in ketamine-anesthetized animals. Images of surface vasculature were acquired using green LED illumination (540 nm) and intrinsic signals were recorded (27 Hz) using red illumination (615 nm). Each trial consisted of 1 s baseline followed by 2 s odor exposure (15-20 trials for each odor). Images (1280 × 1024) of reflectance (R) from the baseline period were summed and subtracted from the average image during the odor period. These images (dR/R) were Gaussian blurred (100 pixel radius) to produce images for subtraction of diffuse odor-evoked reflectance and subsequently median filtered (20 pixel radius).

Supplementary Material

Refer to Web version on PubMed Central for supplementary material.

Acknowledgements

We are very grateful to Andy Peters for his help with 2-photon imaging and contributing analysis software. James Sturgill and Jeff Dahlen gave helpful advice on data acquisition. We thank L.L. Looger, J. Akerboom, D.S. Kim, and the GENIE Project for making GCaMP available and D.F. Albeanu for communication prior to submission. This work was supported by grants from Japan Science and Technology Agency (PRESTO), Pew Charitable Trusts, David & Lucile Packard Foundation, and New York Stem Cell Foundation to T.K., NIH F31DC012698 (A.M.B.), NIH RO1DC04682 (J.S.I.), and NIH R21DC012641 (T.K. and J.S.I.). T.K. is a NYSCF- Robertson Investigator andH.K.K. is a JSPS Postdoctoral Fellow for Research Abroad.

References

Arevian AC, Kapoor V, Urban NN. Activity-dependent gating of lateral inhibition in the mouse olfactory bulb. Nat. Neurosci. 2008; 11:80–87. [PubMed: 18084286]

Boyd AM, Sturgill JF, Poo C, Isaacson JS. Cortical feedback control of olfactory bulb circuits. Neuron. 2012; 76:1161–1174. [PubMed: 23259951]

Briggs F, Usrey WM. Emerging views of corticothalamic function. Curr. Opin. Neurobiol. 2008; 18:403–407. [PubMed: 18805486]

Cazakoff BN, Lau BYB, Crump KL, Demmer HS, Shea SD. Broadly tuned and respiration-independent inhibition in the olfactory bulb of awake mice. Nat. Neurosci. 2014; 17:569–576. [PubMed: 24584050]

Chen T-W, Wardill TJ, Sun Y, Pulver SR, Renninger SL, Baohan A, Schreiter ER, Kerr RA, Orger MB, Jayaraman V, et al. Ultrasensitive fluorescent proteins for imaging neuronal activity. Nature. 2013; 499:295–300. [PubMed: 23868258]

Ghosh S, Larson SD, Hefzi H, Marnoy Z, Cutforth T, Dokka K, Baldwin KK. Sensory maps in the olfactory cortex defined by long-range viral tracing of single neurons. Nature. 2011; 472:217–220. [PubMed: 21451523]

He J. Corticofugal modulation of the auditory thalamus. Exp. Brain Res. 2003; 153:579–590. [PubMed: 14574430]

Kato HK, Chu MW, Isaacson JS, Komiyama T. Dynamic sensory representations in the olfactory bulb: modulation by wakefulness and experience. Neuron. 2012; 76:962–975. [PubMed: 23217744]

Luskin MB, Price JL. The topographic organization of associational fibers of the olfactory system in the rat, including centrifugal fibers to the olfactory bulb. J. Comp. Neurol. 1983; 216:264–291. [PubMed: 6306065]

Markopoulos F, Rokni D, Gire DH, Murthy VN. Functional properties of cortical feedback projections to the olfactory bulb. Neuron. 2012; 76:1175–1188. [PubMed: 23259952]

Matsutani S. Trajectory and terminal distribution of single centrifugal axons from olfactory cortical areas in the rat olfactory bulb. Neuroscience. 2010; 169:436–448. [PubMed: 20457224]

McAlonan K, Cavanaugh J, Wurtz RH. Guarding the gateway to cortex with attention in visual thalamus. Nature. 2008; 456:391–394. [PubMed: 18849967]

Miyamichi K, Amat F, Moussavi F, Wang C, Wickersham I, Wall NR, Taniguchi H, Tasic B, Huang ZJ, He Z, et al. Cortical representations of olfactory input by trans-synaptic tracing. Nature. 2011; 472:191–196. [PubMed: 21179085]

Mombaerts P, Wang F, Dulac C, Chao SK, Nemes A, Mendelsohn M, Edmondson J, Axel R. Visualizing an olfactory sensory map. Cell. 1996; 87:675–686. [PubMed: 8929536]

Murphy PC, Duckett SG, Sillito AM. Feedback connections to the lateral geniculate nucleus and cortical response properties. Science. 1999; 286:1552–1554. [PubMed: 10567260]

Peters AJ, Chen SX, Komiyama T. Emergence of reproducible spatiotemporal activity during motor learning. Nature. 2014; 510:263–267. [PubMed: 24805237]

Petreanu L, Gutnisky DA, Huber D, Xu N, O'Connor DH, Tian L, Looger L, Svoboda K. Activity in motor-sensory projections reveals distributed coding in somatosensation. Nature. 2012; 489:299–303. [PubMed: 22922646]

Rinberg D, Koulakov A, Gelperin A. Sparse odor coding in awake behaving mice. J. Neurosci. 2006; 26:8857–8865. [PubMed: 16928875]

Rothermel M, Wachowiak M. Functional imaging of cortical feedback projections to the olfactory bulb. Front. Neural Circuits. 2014; 8:73. [PubMed: 25071454]

Rubin BD, Katz LC. Optical imaging of odorant representations in the mammalian olfactory bulb. Neuron. 1999; 23:499–511. [PubMed: 10433262]

Shepherd, GM.; Chen, WR.; Greer, CA. The Olfactory Bulb.. In: Shepherd, GM., editor. The Synaptic Organization of the Brain. Oxford University Press, USA; New York: 2004. p. 719Shepherd, G.M., Chen, W.R., and Greer, C.A. (2004) G.M. Shepherd, ed. (New York: Oxford University Press, USA), p. 719

Soucy ER, Albeanu DF, Fantana AL, Murthy VN, Meister M. Precision and diversity in an odor map on the olfactory bulb. Nat. Neurosci. 2009; 12:210–220. [PubMed: 19151709]

Steriade M. Sleep, epilepsy and thalamic reticular inhibitory neurons. Trends Neurosci. 2005; 28:317–324. [PubMed: 15927688]

Stettler DD, Axel R. Representations of odor in the piriform cortex. Neuron. 2009; 63:854–864. [PubMed: 19778513]

Temereanca S, Simons DJ. Functional topography of corticothalamic feedback enhances thalamic spatial response tuning in the somatosensory whisker/barrel system. Neuron. 2004; 41:639–651. [PubMed: 14980211]

Wachowiak M, Economo MN, Díaz-Quesada M, Brunert D, Wesson DW, White JA, Rothermel M. Optical dissection of odor information processing in vivo using GCaMPs expressed in specified cell types of the olfactory bulb. J. Neurosci. 2013; 33:5285–5300. [PubMed: 23516293]

Wiechert MT, Judkewitz B, Riecke H, Friedrich RW. Mechanisms of pattern decorrelation by recurrent neuronal circuits. Nat. Neurosci. 2010; 13:1003–1010. [PubMed: 20581841]

Willhite DC, Nguyen KT, Masurkar AV, Greer CA, Shepherd GM, Chen WR. Viral tracing identifies distributed columnar organization in the olfactory bulb. Proc. Natl. Acad. Sci. U. S. A. 2006; 103:12592–12597. [PubMed: 16895993]

Zhan C, Luo M. Diverse patterns of odor representation by neurons in the anterior piriform cortex of awake mice. J. Neurosci. 2010; 30:16662–16672. [PubMed: 21148005]

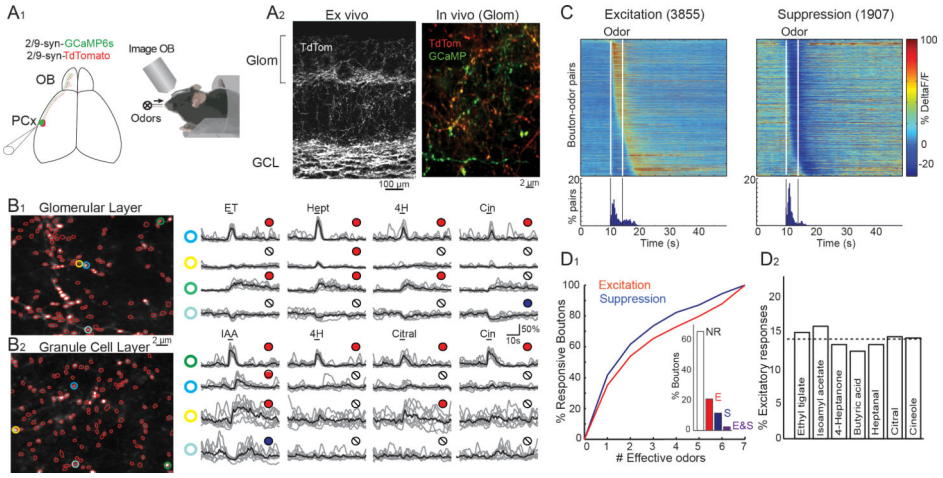

Figure 1. Cortical feedback inputs have diverse response properties

A_1) *Left*, viral vectors expressing GCaMP6s and tdTomato are injected in piriform cortex (PCx) to label olfactory bulb projections. *Right*, schematic of 2-photon imaging via a cranial window over the ipsilateral olfactory bulb (OB) in awake, head-fixed mice. **A_2)** *Left*, tdTomato expression in PCx axons from a coronal OB slice. Axonal projections are most prevalent in the granule cell and glomerular layer. *Right, In vivo* 2-photon image of tdTomato (red) and GCaMP6s (green) expressing boutons from the OB glomerular layer of an awake mouse. **B)** Odor-evoked GCaMP6s activity in individual boutons reveals a wide range of response properties. **B_1)** Responses from a glomerular layer imaging field show that boutons tuned to different odors are intermingled. *Left*, Image of GCaMP6s expression (white) shows ROIs (red outlines) drawn around individual boutons. *Right*, Responses of four boutons (rows) to four odors (columns). Grey lines are individual trails and black lines show the average response to each odor. Filled circles above each trace indicate a significant response (excitation: red, inhibition: blue) and the colored circles to the left of traces indicate ROIs marked in the GCaMP6s image. **B_2)** Responses in the granule cell layer from the same animal. **C)** Dynamics of odor-evoked feedback activity. Top: heat maps of the activity of all responsive bouton-odor pairs showing excitation (3855 bouton-odor pairs) or suppression (1907 bouton-odor pairs), sorted by their onset times (50% of peak). Bottom: histograms of the onset times of all responsive bouton-odor pairs show that excitatory responses are temporally more diverse in the awake state, while inhibitory responses are more time locked to odor onset. Vertical lines indicate the odor period. **D_1)** Odor tuning curve for boutons responding with excitation (red) or suppression (blue). *Inset*, proportion of all boutons with no response (NR), excitation only (E), suppression only (S), or both excitation and suppression (E&S). **D_2)** All odors have an equal probability of eliciting excitatory responses (n = 13 imaging fields). Dashed line indicates expected value (14.3%) if each odor randomly activates boutons with equal probability.

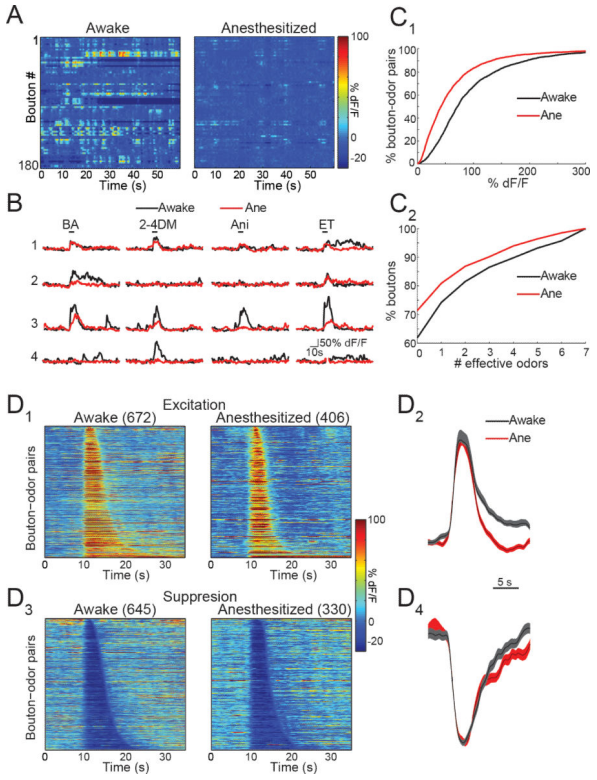

Figure 2. Cortical feedback activity is enhanced during wakefulness

A) Anesthesia reduces spontaneous activity. Heat map of dF/F values for 180 boutons from one imaging field in the awake state (left) and during ketamine anesthesia (right). **B)** Odor-evoked cortical feedback activity is reduced in the anesthetized state. Representative average responses of four boutons (rows) to four odors (black bars) from a single imaging field in the awake (black) and anesthetized state (red). BA; butyric acid, 2-4DM; 2-4 dimethylthiazole, Ani; anisole, ET; ethyl tiglate. **C)** Odor-evoked bouton excitation is stronger (**C_1**) and more broadly tuned (**C_2**) in the awake state. **D)** Odor-evoked excitation is more prolonged in the awake vs. anesthetized state. **D_1)** Heat maps of the activity of bouton-odor pairs showing excitation from the same animals in the awake (left) and anesthetized (right) state, aligned to their onset times and ordered by duration. Numbers of responsive bouton-odor pairs in each condition are in parentheses. **D_2)** Average time course of excitatory responses peak normalized and aligned by their rise times for the awake (black) and anesthetized (red) state. Shading, SEM. **D_3)** and **D_4)** Results for bouton-odor pairs showing odor-evoked suppression.

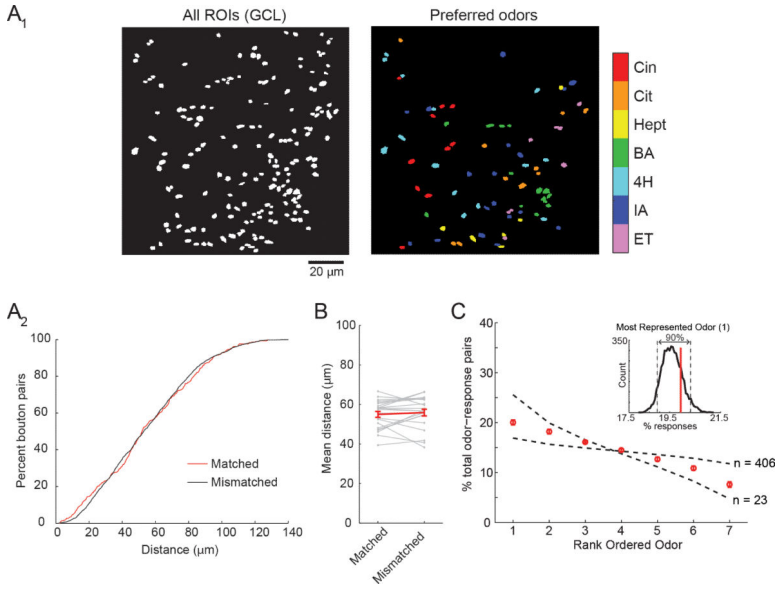

Figure 3. Cortical feedback inputs representing different odors are diffusely distributed at the spatial scale of individual glomeruli

A) Boutons responding to particular odors are not spatially segregated. **A_1)** Results from one granule cell layer imaging field showing all bouton ROIs (left) and map of the preferred odor for each responsive bouton (right). Color scale indicates each of the seven tested odors (Cin; cineole, Cit; citral, Hept; heptanal, BA; butyric acid, 4H; heptan-4-on, IA; isoamyl acetate, ET; ethyl tiglate. ROIs are shown enlarged for clarity. **A_2)** Cumulative frequency distribution of the pairwise distance between all boutons in A_1 with the same (Matched, n=296) or different (Mismatched, n=1702) odor preference. The two distributions are not significantly different (p=0.29, KS test). **B)** Summary data (grey, n=22 fields) reveals no significant difference in the mean distance between matched and mismatched responsive boutons (red, average±SEM). **C)** Rank-ordering orders by their probability of eliciting excitatory responses in individual imaging fields indicates that the fraction of responses elicited by any odor is random. Red circles, responses to rank ordered odors for both granule cell layer and glomerular imaging fields (mean ± SEM, n = 22 fields). The observed values fall within the curves expected by chance for the largest (n=406) and smallest (n=23) number of responsive boutons per imaging field (dotted lines). Inset, response probability distribution for the most represented odor (Odor #1) derived from random subsampling using the sample sizes from 22 imaging fields. Experimentally measured probability (red line) falls within central 90% of the distribution (dotted lines).

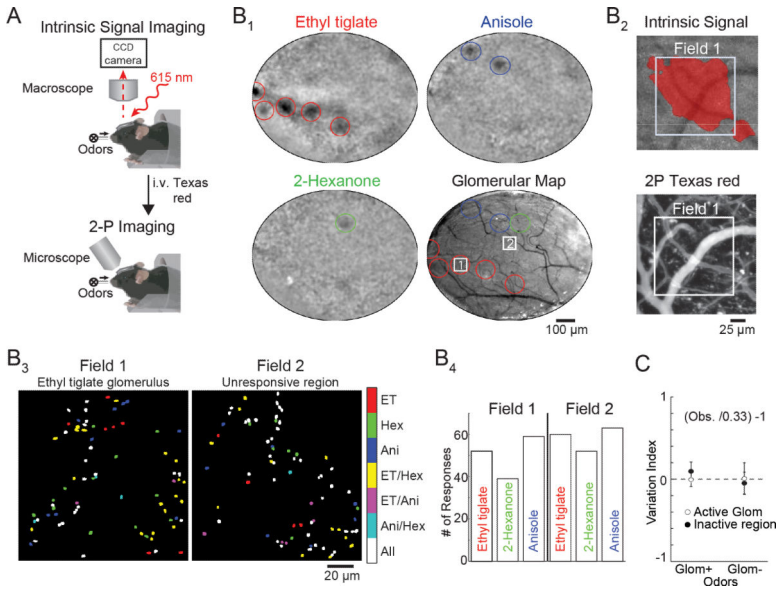

Figure 4. Glomerular layer targeting of feedback inputs is unrelated to glomerular odor specificity

A) Schematic. **B_1)** Intrinsic signal optical imaging from one mouse showing glomerular responses to three different odors (Ethyl tiglate (ET), Anisole (Ani), 2-Hexanone (Hex)) and the activity map superimposed on the olfactory bulb surface vasculature (bottom right). Colored circles highlight activated glomeruli; boxes represent fields selected for bouton imaging. Field 1 is centered over a glomerulus responding to ethyl tiglate and Field 2 indicates a region without a response to the odors. **B_2)** Targeted 2-photon imaging beneath an identified glomerulus. Top, blow up of region around Field 1 from B_1 showing overlay of intrinsic optical signal (red, ethyl tiglate) and surface vasculature. Bottom, 2-photon image stack of Texas red dextran-filled vessels aligned with the vasculature in the image above. **B_3)** Map of glomerular layer boutons responding with excitation within fields indicated in B_1. Colors indicate boutons responding selectively to individual odors (red, green, blue), boutons with overlapping responses to two odors (yellow, magenta, cyan), and boutons responsive to all three (white). ROIs are shown enlarged for clarity. **B_4)** Numbers of boutons responding with excitation to each odor for the fields in B_3. **C)** Summary of results (mean ± SEM) from all experiments using three odors indicates that individual odors were equally likely to activate boutons regardless of the responses of the overlying glomerulus. We calculated a variation index for each odor ((Observed fraction of responsive boutons / 0.33) – 1) for fields centered on an odor-responsive glomerulus (white circles) and fields within regions that did not show a glomerular response to any of the three odors (black circles). Variation index=0 if each odor (1 out of 3) has an equal probability of eliciting bouton responses in an imaging field. Odors were grouped between those that did (Glom+) or did not (Glom-) activate the odor-responsive glomerulus. In all cases, odors consistently had a variation index near zero.